Thermodynamic Simulations of Heat Exchangers for Galley Cooling Regarding Ice Formation

DI Bruno Wiesler, Dr. rer. nat. Robert Kouba, FH JOANNEUM GmbH, Graz, Austria

ABSTRACT

The characteristics and features of aircraft are increasingly defined by means of computer simulations before the first flight. Traditional and advanced testing is still an indispensable complement to computational methods, as a number of physical phenomena have been of a complexity level prohibiting reliable predictions up to now. Those include the frost formation occurring in aircraft internal flows of cooling systems for galleys and trolleys.

Consequently a project was set up for exploring the prospects and improving the abilities of simulation. CFD of the actual status is applied to the heat exchangers of the air cooling units for the identification of already solvable issues and limitations. A commercial CFD software, available in the aviation industries and universities, is extended by models for frost formation.

Finally best practice methodologies for the simulation of the heat exchangers of the air cooling units including frost formation are proposed. The methodology in respect to accuracy, stability and computational efforts is applicable to development processes of aircraft components.

1. INTRODUCTION

The characteristics and features of aircraft are increasingly defined by means of computer simulations before the first flight. Structural analysis, computational fluid mechanics and flight mechanics simulations are examples of well established methods, frequently used in modern aircraft development. The advantages of such simulations are unquestionable. Already at a very early stage of a product development process the functionality and the dimensions of parts can be defined before any hardware is produced. In comparison to experiments, simulation results are by far more detailed, enabling a comprehensive interpretation of physical processes. A technical, economical and ecological optimum can be found in short time at reasonable costs.

Traditional and advanced testing, however, is still an indispensable complement to computational methods, as a number of physical phenomena have been of a complexity level prohibiting reliable predictions up to now. Those include the frost formation occurring in aircraft internal flows of supplemental cooling systems. Briefly the functionality of the systems is described as follows.

Aircraft are equipped with supplemental cooling systems to maintain the quality of the meals and drinks, served to passengers during long distance flights. Regulations of national authorities, are established in order to guarantee the freshness of onboard food and to prevent passengers from possible health threats. The fulfillment of regulations requires the compliance of upper and lower temperature limits during the entire catering chain, e.g. the cooling temperature must not exceed 4 ^{o}C. The supplemental cooling systems, built to keep the temperatures within the given limits, are designed as two independent loops for the reduction in risk of total failure. Each loop contains a centralized equipment, often placed in the belly fairings. Core of this equipment is a chiller, which produces coldness and regulates the temperature of the cooling fluid. The cooling fluid is distributed by means of pumps in a system of ducts, throughout the aircraft to the air coolers. The cooling fluid enters the air coolers' heat exchangers normally at temperatures below 0 ^{o}C. The air coolers are mounted within the galleys and regulate the temperature of the air in the galleys or directly in the trolleys. The air in the galleys may contain water vapor, leading to frost formation at the fins of the air coolers' heat exchangers.

2. THEORETICAL BACKGROUND

Whenever moist air comes into contact with a surface whose temperature is below the dew point temperature of water vapor in air, moisture will condense on the surface. Alternatively, if the surface temperature is below freezing, frost will form. If viewed in the context of refrigeration and air conditioning, the phenomenon of frost formation can have a significant adverse effect on the heat transfer and pressure drop within the systems concerned. For instance, frost formation on heat exchanger surfaces can be extremely detrimental to their operation for several reasons. First, the frost will act as a thermal insulator, thus reducing the ability of the surface to transfer heat to the refrigerant. If there is not a continuous adjustment of the cooling capacity, the heat removed from the refrigerated area will decrease as a function of time, with a resultant change of air condition. Second, the accumulation of frost often becomes thick enough to significantly influence the air resistance of the air cooler coils and/or fins. Consequently, the airflow rate will decrease in time, dependent on the characteristics of the applied fan in the system. If stable cooling and flow conditions are to be kept, the energy demand for the operation of the fan system will increase. Third, to avoid a complete blockage of the air passages, the accumulated frost needs to be removed regularly by a defrosting process. This implies, on the one hand, a non-continuous operational pattern of

the cooling system, and, on the other hand, the necessity to supply additional heat for the melting process in the refrigerated area.

2.1. Stages in the Frost Growth Process

The process of frost formation can be divided into several stages, depending on the aggregate state and structure of the growing frost layer.

First, when water vapor from an air stream starts to be deposited on a frost-free surface at subfreezing temperatures above –40°C, it will usually not directly solidify (desublimate) into ice crystals (Luer (1998), Sanders (1974)). Instead, small distributed spherical water droplets in a sub-cooled state are formed, which will grow in time by further vapor deposition and by coalescence. This initial period, which has theoretically been analyzed by the application of heterogeneous nucleation theory (Fletcher (1970), Sanders (1974), Na and Webb (2003)), is called the drop-wise condensation period (Irragory et al., 2004). It ends after a characteristic time scale t_c, when the droplets distributed over the surface will abruptly solidify (Seki et al., 1985), turning into small dotted ice particles. The time scale t_c is a function of ambient conditions (temperature, type of convection) and surface conditions (temperature and surface roughness). At this point, the particles can be characterized by a mean diameter d and a mean length scale of the respective nucleation site L. The latter basically indicates the mean distance between adjacent ice particles. On the basis of these two parameters, an areal fraction for the solidified droplets (Iragorry et al., 2004) can be defined, which is a significant quantity to describe and model the onset of the next stage in the growth process, which is called the solidification and tip-growth (STG) period (Iragorry et al., 2004). It begins with an isolated one-dimensional growth process (crystal growth period) for each nucleation site. Phenomenologically it appears that each ice particle accumulates matter primarily by extending itself into the linear dimension perpendicular to the cooled surface. This behavior has inspired the development of a small number of simple one-dimensional ice column growth models (Sahin (1995), Tao and Besant (1993a), Tao et al. (1993b)). Next, these isolated rod-type crystals change their shape by the generation of branches around their upper sections, thereby enhancing the three-dimensional character of their structural appearance (Hayashi et al., 1977a). At the same time, these evolving tree-like structures start to interact with each other leading to the formation of a three- dimensional frost layer. The STG period comes to an end when the frost layer appears globally homogeneous and adopts the fundamental properties of a porous medium. It will then be composed of an ice matrix with spaces (pores) being filled with humid air. It is important to mention that the characteristic processes of the STG period are dependent on flow conditions (natural or forced convection) and, hence, the description given above offers only an idealized picture of the situation. For instance, in the case of natural convection the one-dimensional growth pattern is clearly observable (needle shapes), whereas in the case of forced convection it might be largely replaced by the tree-growth pattern (Iragorry et al. (2004), Hayashi et al. (1977a)). Additionally, due to the high diversity and complexity of the evolving structure, little quantitative information is available on the scale of the transitional times in which the different growth patterns of the STG period prevail.

In the next stage, which is termed the densification and bulk growth (DBG) period, the porous character of the frost layer does not change significantly. Accordingly, the temporal effect of the deposited water vapor is twofold. First, a part of it directly solidifies on the frost surface, increasing its thickness. Second, the remaining part will diffuse into the layer and solidify within the pores, thereby increasing the local and mean frost density. The growing frost layer is accompanied by an increasing thermal resistance, which will gradually increase the surface temperature until it reaches the melting point and starts to liquefy the surface frost layer. The resultant water soaks into the porous frost structure and freezes again in lower frost layers, where subfreezing conditions still prevail. This process, which is termed melt-back (see for instance Luer (1998) and Trammel et al. (1968)), causes a sudden increase in the frost layer density and a sudden decrease in its thermal resistance. Consequently, the surface temperature will again drop below the melting point, and the process of desublimation and frost deposition occurs again. This cyclic process of melting, freezing, and deposition will now continue periodically, until an equilibrium condition of heat transfer is reached. During this period, the frost layer becomes a dense and tight structure and ripens into aged frost. The frost growth process is then complete.

2.2. General Assumptions

The fundamental mathematical aspects of the model approach presented here are based on the publication of Na and Webb (2004b).

The model is based on the following assumptions:

1) On the basis of the phenomenological observations described in the previous chapter, the DBG period follows the STG period in time and assumes a ‘closed’ (contiguous) frost layer with a porous structure. For the beginning of the DBG period, a starting value for the frost density of the layer has to be provided. During the subsequent growth process, the density of the continuously renewing frost surface is assumed to be equal to the density of the frost surface layer.

2) Within the frost layer, temperature gradients perpendicular to the cooling wall prevail and are accompanied by respective gradients in vapor pressure. The former ones are the driving potentials for the transport of sensible and latent heat to the cooled wall, whereas the latter ones are responsible for the internal vapor transport through the process of molecular diffusion. Temperature gradients in wall-parallel directions are assumed to be small, and thus transport processes in these directions are negligible. Consequently, the underlying transport equations (differential equations) are spatially one-dimensional.

3) The essential physical parameters for the transport process are the thermal conductivity (heat transport) and the effective diffusion coefficient (mass transport) of the frost layer. Both quantities are closely related to the density of the frost layer. The model thus requires a functional relation between these transport coefficients and the porosity of the layer.

4) Knudson diffusion is neglected. This can be justified by the assumption that the magnitude of the pore diameters is some orders of magnitude larger than the pore dimension where Knudson diffusion begins to play a role.

5) The water vapor is treated by the ideal gas law. The relation between the local vapor pressure and local temperature in the frost layer is given by the saturation curve of water vapor above ice. It is assumed that this relation also applies to the vapor concentration on the frost surface layer. Consequently, effects of a possible super-saturation at the interface between the frost layer and the ambient air stream are not considered. This is a fundamental modification to the work of Na and Webb (2004b).

6) It is assumed that the densification of the frost layer is caused by a spatially continuous solidification process of the internal water vapor over the frost layer thickness. Strictly speaking the spatial continuity of this process is an approximation to the actual physical situation, where deposition can only take place at certain locations (pores) of the layer.

7) The heat transport by radiation in the frost layer can be neglected. The same is assumed for the heat transport by free convection in the pores of the frost layer. Small spatial temperature differences and small radii of the pores justify these assumptions.

These assumptions lead to a set of one-dimensional partials differential equations for heat and mass transfer, which requires a numerical solution procedure.

Additionally certain simplifications and assumptions can be applied, which have been introduced by Sanders (1974) and Le Gall et al. (1997) for the same type of modeling approach (differential analysis).

Various possibilities to simplify the transport equations for energy and mass and have been explored and published in the past (see, for instance, Iragorry et al. (2004)). Most of them focus on the densification process, where either further restrictive assumptions are made on how the water vapor solidifies within the layer, or explicit functional relations to evaluate the frost density are employed. The first approach is applied in the models developed by Jones and Parker (1975) and Lee et al. (1997), and the second approach in the context of the works presented by Cheng and Cheng (2001) and Fossa and Tanda (2005). The model of Jones and Parker (1975) was selected for further considerations, as it offers a good compromise between required numerical efforts and physical details.

2.3. Model Approach

The key issue in the approach developed by Jones and Parker (1975) is the assumption of a uniform densification process within the frost layer. This is based on an explicit algebraic equation for the vapor diffusion rate which offers the possibility of integrating the heat conduction equation analytically. The time dependent frost density can thus be calculated only as a height-averaged mean value. Additionally to the general assumptions, the effective diffusion coefficient D_{eff} for the frost surface has to be modeled in this approach.

Mass transfer
At the surface of the frost layer, the total mass flux given by

$$\dot{m}_{tot} = h_M(\rho_{v,a} - \rho_{v,s}) \tag{1}$$

splits into a densifying part m'_{fd} and a part m'_{fi} which thickens the layer:

$$\dot{m}_{tot} = \dot{m}_{fd} + \dot{m}_{fi} = \frac{\partial \rho_f}{\partial t} x_s + \frac{\partial x_s}{\partial t} \rho_f \tag{2}$$

The driving potential for the vapor mass flux diffusing into the frost layer is the vapor density gradient at $x = x_s$:

$$\dot{m}_{fd} = D_{eff} \left(\frac{\partial \rho_v}{\partial x} \right)\Bigg|_{x=x_s} \tag{3}$$

Alternatively, m'_{fd} can be expressed as a function of the surface temperature and the temperature gradient at the surface by applying the ideal gas law to equation (3) and using the chain rule to introduce the derivative with respect to temperature:

$$\dot{m}_{fd} = \frac{D_{eff} M_v}{R T_s} \left(\left(\frac{\partial P_v}{\partial T} \right)\Bigg|_{x=x_s} - \frac{P_v(T_s)}{T_s} \right) \left(\frac{\partial T}{\partial x} \right)\Bigg|_{x=x_s} \tag{4}$$

M_v denotes the molecular mass and $P_v(T)$ the saturation curve of water vapor above ice. Combining equations (3) and (4) yields the following expression for the densification rate:

$$\frac{\partial \rho_f}{\partial t} = \frac{\dot{m}_{fd}}{x_s} = \frac{D_{eff} M_v}{x_s R T_s} \left(\left(\frac{\partial P_v}{\partial T} \right)\Bigg|_{x=x_s} - \frac{P_v(T_s)}{T_s} \right) \left(\frac{\partial T}{\partial x} \right)\Bigg|_{x=x_s} \tag{5}$$

To determine the frost growth rate dx_s/dt, equation (5) is substituted into equation (2) and combined with the total mass flux given in equation (1):

$$\frac{\partial x_s}{\partial t} = \frac{\dot{m}_{fi}}{\rho_f} = \frac{1}{\rho_f} \left(h_M(\rho_{va} - \rho_{vs}) - \frac{D_{eff} M_v}{R T_s} \left(\left(\frac{\partial P_v}{\partial T} \right)\Bigg|_{x=x_s} - \frac{P_v(T_s)}{T_s} \right) \left(\frac{\partial T}{\partial x} \right)\Bigg|_{x=x_s} \right) \tag{6}$$

Heat transfer
Heat transport is driven by the temperature gradient of the frost layer. Additionally, the latent heat released by the newly formed ice mass during densification represents a distributed heat source in the respective steady-state energy conservation equation:

$$k_f \frac{\partial^2 T_f}{\partial x^2} + H_s \frac{\partial \rho_f}{\partial t} = 0 \tag{7}$$

$$k_f \frac{\partial^2 T_f}{\partial x^2} = -H_s \frac{\dot{m}_{fd}}{x_s} \tag{8}$$

Assuming that the thermal conductivity does not change significantly over the range characterizing the layers temperature profile, a differential equation results which can be integrated analytically and leads to a parabolic

temperature profile:

$$T_f(x) = -\frac{1}{2}\frac{H_s \dot{m}_{fd}}{k_f x_s} x^2 + C_1 x + C_0 \tag{9}$$

The boundary conditions needed to determine the integration constants C_1 and C_0 can be specified as follows:

At the cooled wall, the frost temperature is equal to the wall temperature:

$$T_f(x=0) = T_w \tag{10}$$

Additionally, the heat transport at the wall by conduction is equal to the sensible heat convected to the frost surface plus the latent heat from the freezing water vapor on and within the frost layer:

$$\left.\frac{\partial T_f}{\partial x}\right|_{x=0} = \frac{h_H(T_a - T_s) + H_s(\dot{m}_{fi} + \dot{m}_{fd})}{k_f} \tag{11}$$

The temperature profile is then given by:

$$T_f(x) = -\frac{1}{2}\frac{H_s \dot{m}_{fd}}{k_f x_s} x^2 + \frac{h_H(T_a - T_s) + H_s(\dot{m}_{fi} + \dot{m}_{fd})}{k_f} x + T_w \tag{12}$$

and the respective temperature gradient reads

$$\frac{\partial T_f(x)}{\partial x} = -\frac{H_s \dot{m}_{fd}(x_s)}{k_f x_s} x + \frac{h_H(T_a - T_s) + H_s(\dot{m}_{fi} + \dot{m}_{fd})}{k_f} \tag{13}$$

To calculate the frost growth rate (equation (6)) and the rate of densification (equation (5)) expressions (12) and (13) have to be evaluated at $x=x_s$. This cannot be done explicitly, since the mass fluxes on the rhs of (12) and (13) are themselves functions of surface temperature and surface temperature gradient. However, a solution can be reached through an iterative numerical scheme to evaluate equations (1), (4), (12) and (13) self-consistently.

Remark
In the original work of Jones and Parker (1975), the term $-P_v(T_s)/T_s$ on the right-hand side of equation (4) is neglected without justification. As it is easily included in the formalism, and since it is part of the correct result when applying the ideal gas law and the chain rule to equation (3), it is kept in the present study.

2.4. Numerical Implementation

For the numerical implementation of the model in the CFD system ANSYS CFX (ANSYS-CFX, 2007), the following specific input data and empirical correlations have been selected:

1) Equation to determine the partial pressure P_v of saturated water vapor and the temperature derivative dP_v/dT for subfreezing temperatures (see for instance Hagentoft (2001)):

$$P_v = a \cdot \left(b + \frac{(T - 273.15)}{100}\right)^n \tag{14}$$

$$a = 4.689\ Pa \quad b = 1.486 \quad n = 12.3$$

$$\frac{dP_v}{dT} = \frac{n \cdot a}{100} \cdot \left(b + \frac{(T - 273.15)}{100}\right)^{(n-1)} \tag{15}$$

2a) Equation to determine the average Nusselt number for laminar flow over a flat plate (see for instance Incropera and DeWitt (2002)):

$$Nu = 0.664 \cdot \mathrm{Re}^{1/2}\ \mathrm{Pr}^{1/3} \tag{16}$$

2b) Equation to determine the average Nusselt number for turbulent flow in a parallel plate geometry under frosting conditions based on experimental work by O'Neal and Tree (1984) and Yamakawa et al. (1972):

$$Nu = 0.034 \cdot \mathrm{Re}^{0.8} \tag{17}$$

3) Lewis analogy to calculate the average mass transfer coefficient from the heat transfer coefficient (Incropera and DeWitt (2002), Fossa and Tanda (2005)):

$$h_M = \frac{h_H D_s}{k_{air}} Le^{1/3} = \frac{Nu \cdot D_s}{L_{ch}} Le^{1/3} \tag{18}$$

where the Lewis number Le is given by:

$$Le = \frac{a_{air}}{D_s} \tag{19}$$

The thermal conductivity k_{air}, the thermal diffusivity a_{air} and the diffusion coefficient D_s are all evaluated at the film temperature $(T_s+T_a)/2$. According to Lee et al (1997) the Lewis number is concentrated in a range from 0.7 to 1.0.

4) Diffusion coefficient D of water vapor within dry air (Le Gall et al., 1997):

$$D = 1.451 \times 10^{-4} \frac{T^{1.72}}{P_t} \tag{20}$$

where P_t denotes the total pressure of the air/vapor mixture.

5) Effective diffusion coefficient according to Auracher (1972):

$$D_{eff} = \left(\frac{1 - f_{ice}}{1 - 0.58 \cdot f_{ice}}\right) D_s \tag{21}$$

6) Thermal conductivity as a function of frost density according to Sanders (1974):

$$k_f = 1.202 \cdot 10^{-3} \rho_f^{0.963} \tag{22}$$

or alternatively by Lee et al (1994):

$$k_f = 0.132 + 3.13 \cdot 10^{-4} \rho_f + 1.6 \cdot 10^{-7} \rho_f^2 \tag{23}$$

7) Initial values for frost thickness (x_s) and frost density (ρ_f). The values are based on numerical investigations made by Na and Webb (2004b), Le Gall (1994), Le Gall et al. (1997), Jones and Parker (1975).

$$x_s(t=0) = 5 \cdot 10^{-5}\ m \qquad \rho_f(t=0) = 30\ kg/m^3 \tag{24}$$

2.5. Refinement of the Properties at the Surface of the Frost Layer

First applications of the model and the empirical correlations reveal deviances between the simulation and experimental findings and need to be investigated. Deficiencies in heat and vapor mass transfer to the frost surface probably overlap with some of the DBG model. As they are apparently the major source of deviances between experimental and simulation results, further investigations are focused on the improvement of mass and heat transfer. In this respect the enhancement of the heat and vapor mass fluxes to the frost surface are identified as the essential quantity to significantly improve the accuracy of frost growth calculation.

The first CFD simulations so far are performed under the assumption of hydraulically smooth walls. In comparison to rough walls, as occurring at the frost surface, the heat and mass transfer is obviously under predicted.

According to O'Neal and Tree (1985) the average heat transfer for turbulent flows due to a frost layer is enhanced by approximately 60% when compared to a Dittus-Boelter-relationship, which represents hydraulically smooth conditions.

According to Lee et al (1997) the Lewis numbers are concentrated between 0.7 and 1 for humid air flow/frost interfaces. A value of Le = 0.8 is considered a standard value in the first CFD simulations. With

$$D_s = \frac{a_{air}}{Le} = \frac{k_{air}}{\rho_{air} c_{p,air} Le} \tag{25}$$

the mass transfer is inverse proportional to the Lewis number and thus the mass transfer enhances for smaller Lewis numbers.

In CFD, in particular in CFX, the heat transfer coefficient at the boundary cannot be influenced directly. For relatively large computational grid cells at the surface with a center located in the turbulent sublayer of the boundary layer the heat flux is calculated according to Kader (1981). If the center of the cell adjacent to the wall is within the laminar sublayer, a linear velocity and temperature profile is assumed. The heat flux is calculated from the thermal conductivity and the temperature gradient at the wall.

CFX recommends small cells for the simulation of heat transfer with the cell centers located in the laminar sublayer to avoid presumed velocity (and temperature) profiles. It has to be pointed out, that in all simulations performed for this work, the recommendations are regarded.

However, instead of a direct determination of the heat transfer coefficient, the thermal conductivity k of the fluid can be increased to cause a heat transfer enhancement. A series of simulations are performed to adjust the thermal conductivity to achieve an increase of 60% in heat transfer at the interface humid air/frost layer. A factor of 1.96 turned out to be the appropriate choice for the consideration of the influence of the rough frost layer on heat transfer:

$$k_{air\ frost} = 1{,}96\ k_{air} \tag{26}$$

Further improvements in the accuracy of the simulations are achieved by setting Le = 0.7. The diffusion coefficient is increased in total by both measures by a factor of 2.24:

$$\frac{D_{s\ frost}}{D_s} = \frac{k_{air\ frost}\ Le}{k_{air} Le_{new}} = 2{,}24 \tag{27}$$

The final adjustment affects the thermal conductivity of the frost layer. A decision, which of the correlations, available in literature, represents the situation best, cannot be made on the basis of available experimental data. Thus again a series of simulations is conducted. Best results are obtained when the calculation of the thermal conductivity is performed as a mean of the correlation according to Sanders (1974), equation (30), and of the correlation according to Lee et al. (1994), equation (31) and as follows:

$$k_{f\ new} = 0{,}5\ (k_{f,Sanders} + k_{f,Lee}) \tag{28}$$

2.6. Model Validation

The validation test case for the CFD implementation refers to the experimental investigations of Mao et al. (1999), which were carried out in the turbulent flow regime. The experiments are performed with a cooled flat rectangular plate, which is mounted in a rectangular channel and which is exposed to a humid air stream at sub-freezing temperatures.

The results obtained with refined approach are displayed form Fig. 1 to Fig. 4. in comparison to the experimental results and the results obtained with the basic simulations without refinement.

The frost growth is significantly increased with the refined approach. After 90 minutes the layer thickness is calculated to be x_s=1.16 mm (exp. correlation: x_s=1.13 mm, basic simulation: x_s=0.63 mm) and the density is ρ_f=79 kg/m^3 (exp. correlation: ρ_f=84 kg/m^3 , basic simulation: ρ_f=115 kg/m^3). The corresponding values for the total frost mass are m_f = 9.1 kg/m^2 (refined approach, basic simulation: 7.3 kg/m^2) and m_f = 9.5 kg/m^2 (exp. correlation) respectively. The total frost mass is thus predicted with an accuracy within 5%.

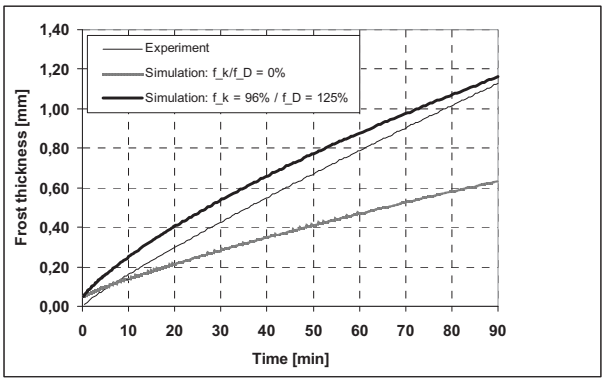

Fig. 1: Comparison of basic and refined model results with experimental data according to Mao et al (1999) of the mean frost thickness over time

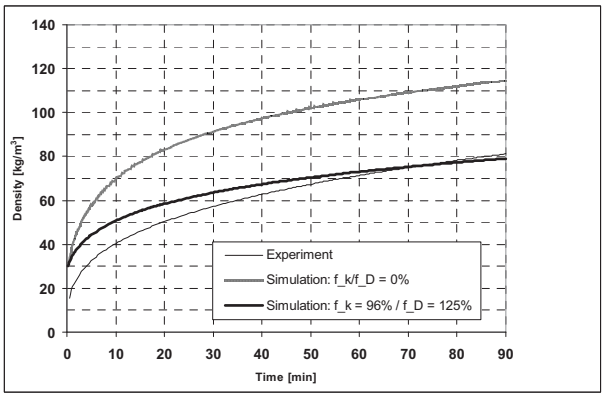

Fig. 2: Comparison of basic and refined model results with experimental data according to Mao et al (1999) of the mean frost density over time

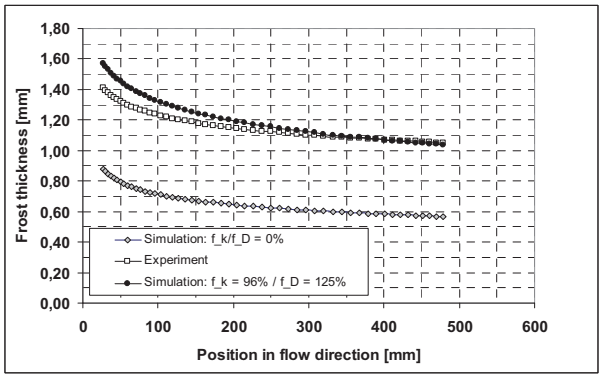

Fig. 3: Comparison of basic and refined model results with experimental data according to Mao et al (1999) of the frost thickness over the plate length after 90 min

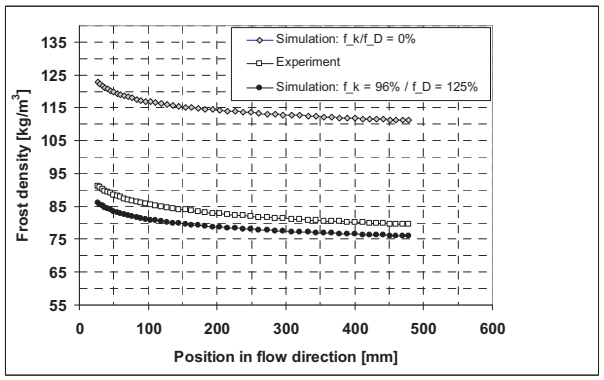

Fig. 4: Comparison of basic and refined model results with experimental data according to Mao et al (1999) of the frost density over the plate length after 90 min

With regard to the spatial frost distribution over the cooling plate the thickness and density shapes are already in good agreement with the experimental data, i.e the relative runs of the curves are very similar. The large offset of the curves indicate inaccurate results. With the refined approach the absolute values of the spatial distribution of frost thickness and frost density are very close to experimental data. The already proper characteristics of the curves are maintained.

For the refined approach for heat and mass transfer at the frost layer surface universal validity cannot be claimed. It is developed on the bases of experimental data, which are rather sparse. The clear influence of the rough frost surface on heat and mass transfers requires modifications of the simulation models, which are originally developed for hydraulically smooth surfaces or other incomparably physical situations. The refined approach is expected to tackle a fundamental problem of the simulations for turbulent flow situations according to means, currently available. More experiments and corresponding modeling and simulations are required to further improve the universality of the approach. As outlined, the refined approach is limited to turbulent flows over frost layers. The improvements in accuracy for laminar flow situations need a similar procedural method.

It can be assumed that both models, for heat and mass transfer as well as for the DBG, cover coherently the required aspects of the underlying physics. Major uncertainties are resulting form the coefficients, h_H and h_M for heat and mass transfer respectively and k_f for the heat conduction and D_{eff} for the diffusivity in the frost layer.

3. APPLICATION OF THE MODELS TO HEAT EXCHANGERS OF A COOLING UNIT

3.1. Preparing CFD Simulations

The geometry and boundary conditions of the heat exchanger are approximated (presumed) according to Zerbes and Schmid (2006). A general sketch of the heat exchanger is depicted in Fig. 5.

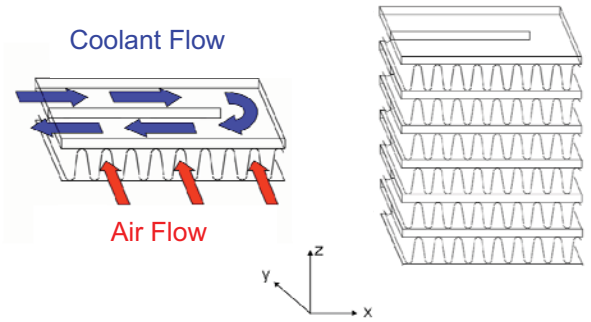

Fig. 5: Principal sketch of the cross-counter flow configuration (adapted from Ebigt, 2003)

The selected simulation domain consists of one coolant flow channel, the corresponding air passages, the solid fins and a solid plate. A representative section of the computational mesh of the heat exchanger element is displayed in Fig. 6.

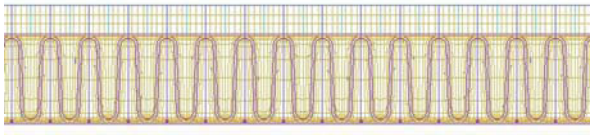

Fig. 6: A representative section of the computational mesh of the heat exchanger element.

The main characteristics of the coolant flow in comparison to water are a higher density (~ 1800 kg/m^3) and kinematic viscosity (~2 ·10^{-6} m^2/s) and a significantly lower thermal conductivity (~7·10^{-2} W/(mK)) and heat capacity (~900 J/(kgK). The resulting Prandtl number is ~45, which is approximately a factor six larger than the one of water

The shell of the duct and the division bar are assumed to be made of aluminum. The main physical properties of the material can be found in Incropera and DeWitt (2002).

A representative operational pattern of the heat exchanger, which is used throughout the CFD calculations, can be summarized as follows:

- Inlet temperature (air side): 277 K
- Inlet velocity (air side): 3,4 m/s
- Inlet temperature (coolant side): 265 K
- Inlet velocity (coolant side): 0,125 m/s

Four variants with variations in the coolant flow channel are calculated (Fig. 7):

- b (basic): No partition walls
- V1: Partition walls in the straight cross flow parts
- V2: 10 Baffles in the straight cross flow parts with a periodicity of 2
- V3: Configuration V2 and partition walls in the counter flow part

The numbers of grid nodes are 2.7 MCells for b and V1, 4.3 MCells for V2 and 9.0 MCells for V3.

Fig. 7 depicts the temperature distributions in the center plane of the coolant channel for the basic simulation and the variants. The influence of the baffles, their enhancement of the heat transfer and their homogenizing effect on the temperature distribution are clearly visible.

Fig. 8 displays the temperature distribution at the air outlet of the fins. The coolant inlet/outlet is on the left hand side of the figures. The cooling performance rapidly drops in case of the basic variant without walls or baffles. The air temperature at the outlet of the fins varies from approx. 273 K (at the coolant inlet/outlet) to 275 K (at the counter-flow region). The cooling performance significantly increases by the usage of partition walls (V1) and baffles (V2) in the cross-flow regions. An air temperature distribution close to uniformity and a drop in temperature level can be achieved by the usage of baffles in all parts of the coolant channel (V3).

An increase of surface heat flux can be recognized with the increase in complexity of the build-in elements from variant to variant.

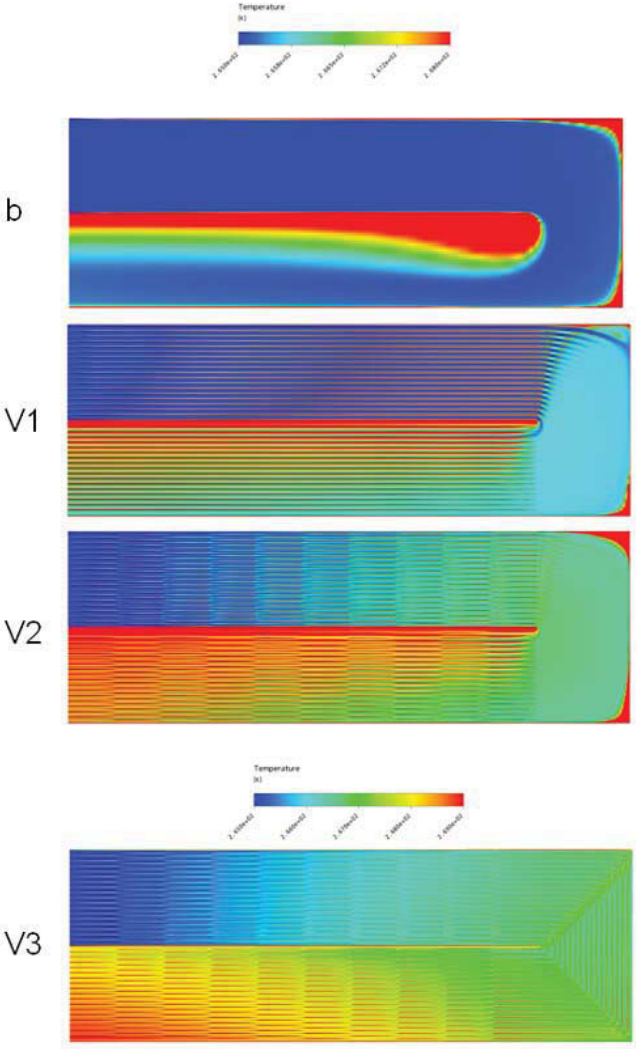

Fig.7: Temperature distributions in the center plane of the coolant channel

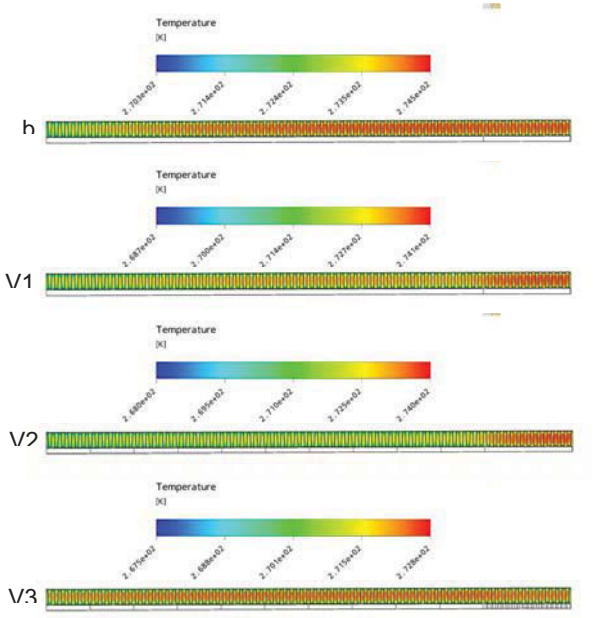

Fig 8: Temperature distribution at the air outlet of the fins

In Fig. 9 the temperature distribution in the coolant inlet and outlet is depicted. In case of the basic variant a large portion of the outgoing coolant still is at the inlet temperature, e.g. the cooling potential is utilized just to a small extend. By the usage of partition walls and baffles, the performance is increased and a nearly uniform distribution at a low temperature level can be achieved (V3).

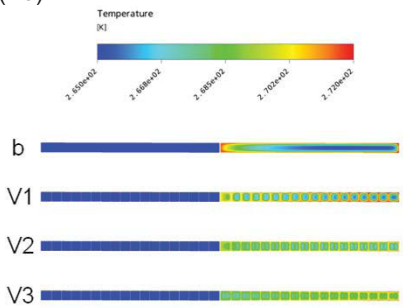

Fig. 9: Temperature distribution at the coolant inlet and outlet

3.2. Best Practice Methodologies

When parameter studies of fin configurations in relation to frost formation are required, it might be sufficient to pick out single air micro channels at locations of interest.

The suggested practice is demonstrated for the heat exchanger for two airside micro channels (Fig. 10). The first position is at the inlet/outlet area of the coolant (fin 1, x=0) and the second position is at fin 60. The boundary conditions are based on simulation V2 of the heat exchanger element. At fin 1 the air flow passes an area where the coolant has the highest and the lowest temperature in the channel. The drop of the air temperature at this fin is at the maximum, compared with the other fins. At fin 60 the coolant temperatures at the air inlet is lower and at the air outlet higher than at fin 1. In total, the temperature drop of the air is lower at fin 60 than at fin 1.

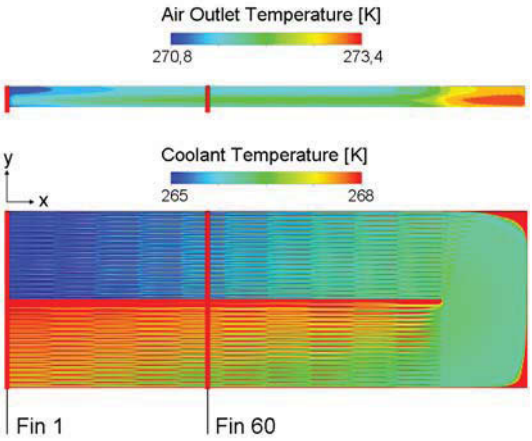

Fig. 10: Positions of the selected airside micro channels

For the simulation of the frost formation, the mesh and the boundary conditions are equal to those described under 3.1, The simulation of the frost formation is started after a converged solution of the conjugate heat transfer setup air/aluminum is achieved.
For frost formation, the model according to Jones and Parker (1975) is used with the refinements described in section 2.5.

At fin 1, where the air is cooled to a lower temperature than at fin 60, the growth rate of the frost layer is higher. After 60 min an average frost height of 0.58 mm is reached, which is about 0.2 mm more than at fin 60.

The distribution of the frost height after 60 min is displayed in Fig. 11. Peak values of more than 1 mm are observable on fin 1 and more than 0.6 mm for fin 60. It has to be remembered, the average values are 0.58 and 0.38 mm, respectively. The massive frost accumulation is in the vicinity of the air outlets and decreases with the number of fins in x-direction. This is in good agreement with experimental experiences (Zerbes, 2008).

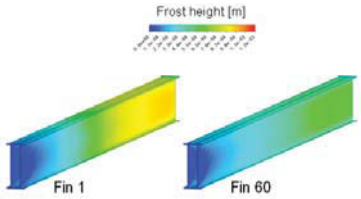

Fig. 11: Distribution of frost height

The distribution of the thermal quantities for fin 1 at the beginning of the frost growth and after 60 min is depicted in Fig. 12. At the beginning of the frost growth process, at t=0, the surface temperature and the sensible heat flux decrease continuously in flow direction. At that time, the conditions are such that the center of desublimation is at the start of the second half of the fin, which is observable in the distribution of the latent heat flux.

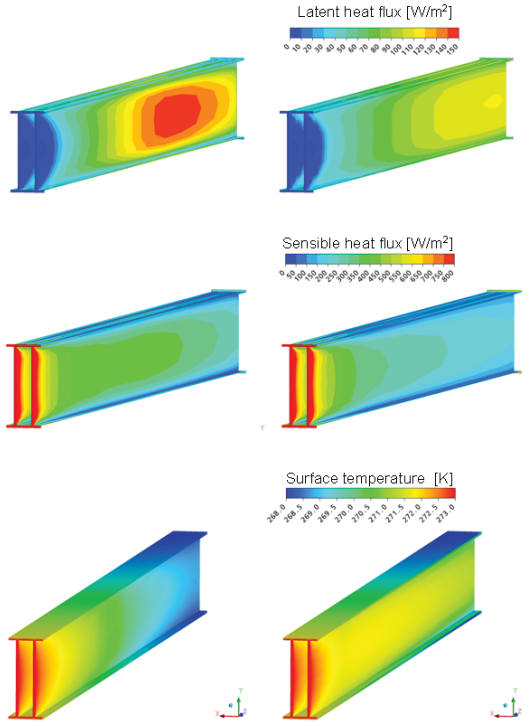

Fig. 12: Distribution of thermal quantities, latent heat, sensible heat flux and surface temperature

The model is capable of reproducing the major features, which occur during the frost deposition:

After 60 min, the surface temperature next to the inlet, in the fist third of the fin, is unchanged, because there is no frost layer growing. The increase in frost layer height in flow direction has an isolation effect. The sensible heat flux decreases and the surface temperature increases compared to the situation at the beginning of the process. The break down of the heat exchanger performance is obvious. Because of the slow down of the cooling process of the air, the desublimation and the rejection of latent heat is shifted downstream to the vicinity of the outlet.

4. SUMMARY

In order to enable 3 dimensional CFD simulations of frost formation in aircraft air systems, in the supplemental cooling system, comprehensive studies are performed. The prevailing processes of frost accretion at heat exchangers of air conditioning units is the desublimation of the air humidity at the cooling fins.

For the simulation of the water vapor deposition and the connected phase change at cold surfaces, models and fluid properties, available in literature, are reviewed. Further on, one model is selected and implemented in a commercial CFD code. A refined approach to regard the influence of the frost surface on heat and mass transfer from the air to the frost layer is proposed.

CFD including the newly developed software is applied elements of heat exchangers of an air cooling unit. Consistent simulation results are achieved. Furthermore, potential for improvements of the simulations models is identified. Accompanying detailed measurements, e.g. of special and temporal frost density, of frost layer thickness, of frost surface temperatures and of heat flux is required.

Best-practice methodologies for the CFD simulations of the aircraft components are suggested. The simulation of the heat exchanger, even without frost formation, may be characterized as a challenge due to the conjugate heat-transfer problem, including the coolant and air flow and the heat transfer in the aluminum and due to geometrical details. Nevertheless, to the authors' knowledge, for the first time a plausible spatial frost distribution on a cooing fin of an air cooling unit could be generated by means of 3D numerical simulation.

5. NOMENCLATURE

D	diffusion coefficient	$[m^2/s]$
h_H	heat transfer coefficient	$[W/m^2K]$
h_M	mass transfer coefficient	[m/s]
H_s	heat of sublimation	[J/kg]
k	thermal conductivity	[W/(m K)]
L	length scale, length, distance	[m]
m	mass	[kg]
$\dot{m}$, m'	mass flux	$[kg/(m^2\ s)]$
M	molecular mass	[kg/kmol]
p	partial pressure	[Pa]
q	heat flux	$[W/m^2]$
R	universal gas constant	[J/(mol K)]
t	time	[s]
T	temperature	[K]
x	distance from wall	[m]
Re	Reynolds number	[-]
Nu	Nusselt number	[-]
Pr	Prandtl number	[-]
Le	Lewis number	[-]

Greek symbols

ρ	density	$[kg/m^3]$
ω	specific humidity	[kg/kg]

Subscrips

eff	effective	eff
f	frost	f
fd	part of the newly formed frost that increases the density of the layer	fd
fi	part of the newly formed frost that increases the thickness of the layer	fi
i	inner	i
loc	local	loc
o	outer	o
s	frost surface	s
tot	total	Tot
v	water vapour	v
w	wall	w

6. REFERENCES

ANSYS-CFX (2007), version 11.0, Copyright 1996-2007 ANSYS Europe LTd.

Auracher, H. (1972): *Water vapor diffusion and frost formation in capillaries*, Annex 1972-1. In Bulletin of the International Institute of Refrigeration, Communications B1, B2, and E1, Freudenstadt, 477-488.

Cheng, C.H., Cheng, Y.C. (2001): *Predictions of frost growth on a cold plate in atmospheric air*, Int. Comm. Heat Mass Transfer **28** (7), 953-962.

Ebigt, W. (2003): *Die dynamische Modellierung eines Luftkühlers für Flugzeugküchen*, Diplomarbeit, Hochschule für Technik Karlsruhe (FH).

Fletcher, N.H. (1970): *The chemical physics of ice*, Cambridge University Press, Cambridge, 1970.

Fossa, M., Tanda, G. (2005): *Modeling of Frost Growth in Simple Geometries and Passages*, Proceedings of the 16th IASTED international conference on modeling and simulation, Cancun/Mexico.

Hagentoft, C.-E. (2001): *Introduction to building physics*; Studentlitteratur AB.

Hayashi, Y., Aoki, K., Adachi, S., Hori, K. (1977a): *Study of Frost Properties correlating with Frost Formation Types*, J. Heat Transfer **99**, 239-245.

Incropera, F.P., DeWitt, D.P. (2002). *Fundamentals of heat and mass transfer*, John Wiley & Sons, New York, 2002.

Iragorry, J., Tao, Y-X., Shaobo J. (2004): *A Critical Review of Properties and Models for Frost Formation Analysis*, HVAC&R Research **10** (4), 393–419.

Jones, B.W, Parker, J.D. (1975): *Frost Formation with Varying Environmental Parameters*, J. Heat Transfer **97**, 255-259.

Kader, B.A. (1981):*Temperature and concentration profiles in fully turbulent boundary layers*, International Journal of Heat and Mass Transfer, 24(9):1541-1544,

Le Gall, R. (1994): *Experimental study and modeling of frost formation in heat exchangers*, Ph.D. thesis, Institut National Polytechnique de Grenoble.

Le Gall, R., Grillot, J.M., Jallut, C. (1997): *Modeling of Frost Growth and Densification*, Int. J. Heat Mass Transfer **40** (18), 3177-3187.

Lee, K.-S., Lee, T..-H., Kim, W.-S. (1994): *Heat and mass transfer of parallel plate heat exchanger under frosting conditions*, SAREK Journal **6**, 155-165.

Lee, K.-S. Kim, W.-S., Lee, T.-H. (1997): *A One-Dimensional Model for Frost Formation on a cold Flat Surface*, Int. J. Heat Mass Transfer **40** (18), 4359-4365.

Luer, A (1998): *Reifbildung an parallelen, gekühlten Platten eines mit feuchter Luft laminar durchströmten Kanals*, Dissertation, Technische Universität Darmstadt, Darmstadt, 1998.

Mao, Y., Besant, R.W., Chen, H. (1999), *Frost Characteristics and Heat Transfer on a Flat Plate under Freezer Operating Conditions*: Part I, Experimentation and Correlations, ASHRAE Transactions **105** (2), 4295-43.

Na, B., Webb, R.L. (2003): *A fundamental understanding of factors affecting frost nucleation*, Int. J. Heat Mass Transfer **46**, 3797-3808.

Na, B., Webb, R.L. (2004b): *New model for frost growth rate*, Int. J. Heat Mass Transfer **47**, 925-936.

O'Neal, D.L., Tree, D.R (1984): *Measurement of Frost Growth and Density in a Parallel Plate Geometry*, ASHRAE Trans. **90**, 278-290.

O'Neal, D.L., Tree, D.R (1985): *A Review of Frost Formation in Simple Geometries*, ASHRAE Trans. **91**, 267-281.

Sahin, A.Z. (1995): An Analytical Study of Frost Nucleation and Growth during the Crystal Growth Period, Int. J. Heat Mass Transfer **30**, 321-330.

Sanders, C.T. (1974): *Frost formation: The influence of frost formation and defrosting on the performance of air-coolers*, Ph.D. thesis, Delft University of Technology, Delft, 1974.

Seki, N., Fukusako, S., Matsuo, K., Uemura, S. (1985): *An Analysis of Incipient Frost Formation*, Wärme- und Stoffübertragung **19**, 9-18.

Tao, Y.-X., Besant, R.W. (1993a): *Prediction of Spatial and Temporal Distributions of Frost Growth on a flat Plate Under Forced Convection,* J. Heat Transfer **115**, 278-281.

Tao, Y.-X., Besant, R.W., Rezkallah, Y. (1993b): *A Mathematical Model for Predicting the Densification and Growth of Frost on a Flat Plate*, Int. J. Heat Mass Transfer **36**, 353-363.

Trammel, G.J., Little, D.C. , Killgore, E.M. (1968): *A Study of Frost Formed on a flat plate Held at Sub-Freezing Temperatures*, ASHRAE J. **10**, 42-47.

Yamakawa, N., Takahashi, N., Ohtani, S. (1972): *Forced convection heat and mass transfer under frost condition.* Heat Transfer Japanese Research **1**, 1-10.

Yonko, J.D., Sepsy, C.F. (1967): *An Investigation of the Thermal Conductivity of Frost While Forming on a Flat Horizontal Plate*, ASHRAE Trans. **73**, Part I, 1-11.

Zerbes, I., Schmid, M. (2006): *private communications*; AOA Gauting and Airbus, Germany

Zerbes, I.,(2008): *private communications*; AOA Gauting, Germany